RSC Publishing Faraday Discussions

Spectroscopy of Temporary Anion States: Renner-Teller Coupling and Electronic Autodetachment in Copper Difluoride Anion

Journal:	*Faraday Discussions*
Manuscript ID	FD-ART-12-2018-000224.R1
Article Type:	Paper
Date Submitted by the Author:	28-Dec-2018
Complete List of Authors:	Lyle, Justin; Washington University in St. Louis, Chemistry Jagau, Thomas; Ludwig-Maximilians-Universitat Munchen, Chemistry Mabbs, Richard; Washington University in St. Louis, Chemistry

Journal Name

ARTICLE

Spectroscopy of Temporary Anion States: Renner-Teller Coupling and Electronic Autodetachment in Copper Difluoride Anion

Received 00th January 20xx,
Accepted 00th January 20xx

DOI: 10.1039/x0xx00000x

www.rsc.org/

Justin Lyle,[a] Thomas-Christian Jagau[b] and Richard Mabbs*[c]

Photoelectron angular distributions determined in small energy increments between 3.522 and 3.650 eV reveal distinctly different detachment mechanisms within the $CuF_2^-(X^1\Sigma_g^+)$ → linear CuF_2 $(X^2\Sigma_g^+)$ + e^- band. Certain channels also display non-Franck-Condon behavior, the action spectra of which reveal rich structure. The behavior reflects excitation to an electronically unbound anion state (at the linear geometry). The effects of the intermediate state are observed in the detachment behavior at photon energies down to the X $^1\Sigma_g^+$ → X $^2\Sigma_g^+$ threshold. Adiabatic CAP-EOM-CCSD (equation of motion coupled cluster singles and doubles, including a complex absorbing potential) energy curves are presented along the bending coordinate, showing the complexity of anion and neutral states for this system. The photodetachment action spectra represent a spectroscopic probe of the vibronic state energies in the vertical excitation region and highlight the need for treatment of vibronic coupling in systems involving the loss of an electron.

Introduction

The excited states of anionic species are often unstable with respect to electron loss and therefore only tend to exist as short lived resonances.[1, 2] These states are of great interest as they represent situations in which a free electron strongly interacts with a neutral molecule. Thus they may act as doorway states for electron capture and therefore chemical reduction pathways, dissociative electron attachment processes and other electron collision/capture induced chemistry.[3-9] However, the inherently unstable nature of these states represents a significant challenge for computation. Methods developed for stationary (bound) states are clearly not recommended and complex variable non-Hermitian methods,[1, 10, 11] for example involving the use of complex absorbing potentials (CAP) are required to deal with such problems.[12-17]

It is desirable to reveal the internal mode structure and equilibrium geometries to provide tests of state-of-the art *ab initio* methods. However, these states also represent a significant experimental challenge. Part of the difficulty lies in producing these transient anions. Electron scattering experiments have revealed a great deal of information over the years. Another promising approach is to start from a stable anionic state and use photoexcitation to access resonances.[18-21] This offers good control over the energetics of the system and charged particle imaging detection schemes[22, 23] allow efficient collection of the ejected electrons. In addition, both the photoelectron energy and angular distributions contain information relating to the interactions occurring in the detachment process and hence represent potentially sensitive probes of the resonances.

The essence of the approach relies on the observation of changes in the photoelectron spectra as a function of excitation energy. In this work we highlight the possibility of using anion photoelectron imaging along with a tunable photon source to reveal details of the internal mode structure of low lying resonances of CuF_2^-. Calculations show that this system has several low-lying anion resonances and the selection rules for direct detachment or electron loss mediated by the presence of a resonance are different. This has recently allowed determination of all vibrational frequencies of the anion and neutral ground states of CuF_2^-.[24]

To establish a framework in which to discuss the results presented herein, brief details of this earlier study are presented in fig. 1. The two representative CuF_2^- photodetachment spectra were recorded at photon energies 3.546 eV (top) and 3.603 eV (bottom). The observed transitions correspond to the energy difference between an initial anion and final neutral level, regardless of the mechanism via which the electron detaches. The feature labelled 0_0^0 is found at the adiabatic electron affinity (3.494 eV) and contains the zero-point to zero-point transition between the anion and neutral ground states. Since the ion source produced relatively hot CuF_2^-, several vibrational levels of the anion ground electronic state were populated. The 0_0^0 feature therefore includes transitions between bending levels with the same number of quanta ($2_{n''}^{n'=n''}$). The feature labelled 1_1^0 represents the first symmetric stretching hot-band from the neutral and the attendant $1_1^0 2_{n''}^{n'=n''}$ series. In addition, there

[a] Chemistry Department, Washington University in St. Louis, St. Louis, Missouri, USA
[b] Department Chemie, LMU München, München, Germany.
[c] Chemistry Department, Washington University in St. Louis, St. Louis, Missouri, USA

are several features which should have negligible Franck-Condon factors (for direct detachment) that are primarily associated with changes in bending quanta, $2^{n'_{n''}=n''+1}_{n}$ (for brevity labelled $2[+1]$), $2^{n'_{n''}=n''+2}_{n}$ ($2[+2]$), and $2^{n'_{n''}=n''+3}_{n}$ ($2[+3]$) to the higher energy side of 0^{0}_{0}, and $2^{n'_{n''}=n''-1}_{n}$ ($2[-1]$) and $2^{n'_{n''}=n''-2}_{n}$ ($2[-2]$) to lower energy. The intensities of these features are strongly dependent on the photon energy, a characteristic of detachment via a transient intermediate anion state.

In this work the photon energy dependence of these features is used to offer a window into resonance internal energy level structure. In principle the resolution of this approach is much better than usually achieved in photoelectron spectroscopic measurements as it is determined by the bandwidth of the excitation pulse. This has been demonstrated before, for example in measurements of the detachment cross section of CH_2CN^- in the vicinity of a dipole bound state. Rotational structure has been recorded[25-27] which more recently has shown the interaction of the CH scissor and umbrella modes in the dipole bound state.[28]

Dipole bound states are actually electronically stable with respect to electron loss, but the electron binding energy (eBE) is sufficiently weak that excitation of one or more vibrational quanta causes electron loss via vibrational autodetachment. In the current work we examine the possibility of extending this approach to probe the internal levels of a resonance state subject to electronic autodeachment, with CuF_2^- constituting an ideal example. Following a brief description of the experimental methods used to produce and probe the CuF_2^- ions we present a summary of the low lying electronic states of this system, calculated using EOM-CCSD methods. Experimental results show how the photoelectron angular distributions depend on the pathways underlying electron loss. Trends in the photoelectron intensities are then discussed in terms of the low lying electronic states identified in the calculations. The results both highlight the possibility of probing the internal modes of low lying anion resonances, while the complexity of the vibronic states shows the need for development of new theoretical models of the role of interstate coupling in autodetachment to interpret the data.

Experimental

Experiments are performed using a custom-built anion photoelectron imaging time-of-flight mass spectrometer (TOF-MS) which has been described in detail elsewhere. [18, 24, 29] The instrument incorporates a DC ion discharge source,[30] Wiley McLaren TOF arrangement[31] and velocity mapped imaging (VMI)[23] lens. The source chamber (1×10^{-5} Torr), TOF-tube (1×10^{-7} Torr) and detection region (5×10^{-9} Torr) are differentially pumped.

A pulsed supersonic expansion of O_2 (backing pressure 40 psig) passes through the DC discharge. The discharge is supported by one stainless steel and one copper electrode which are insulated from the faceplate of the nozzle using Teflon discs. The copper electrode serves as the Cu atom source and the insulators serve as the fluorine atom source. TOF-MS is used to select the $^{63}CuF_2^-$ anion which is photoexcited with a linearly polarized photon pulse from a Nd:YAG (Spectra-Physics INDI-10) pumped dye laser (Spectra-Physics Cobra Stretch) synchronized to coincide with ion arrival at the center of the VMI lens. The photon energies (*hν*) were selected in the range 3.522 – 3.650 eV, with narrow spacings (usually 1 meV) and the duty cycle for the experiment is 10 Hz.

The VMI lens is configured in-line with the anion TOF axis. Ions enter through a 3 mm skimmer and the laser is narrowed to the same dimension using an external iris. Photoelectrons are detected on a 40 mm dia. dual-Chevron MCP/P20 phosphor screen detector (Burle Inc.). Electron impacts are recorded using a CCD camera (IMPERX VGA 120L), centroided[32, 33] and binned (to a workable signal-to-noise limit) yielding an effective 1280×960 pixel grid. The spectral resolution afforded by this arrangement is ΔeKE/eKE = 1.4 % at eKE = 0.6 eV.[34]

Velocity domain spectra are extracted from the images subsequent to BASEX[35] transformation. These are converted to the electron kinetic energy (eKE) or binding energy (eBE) domain using the appropriate Jacobian transformation and energy conservation (eBE = *hν* – eKE). The energy is calibrated for the imaging arrangement using images of F^- (simultaneously produced in the discharge source) which has a distinctive spectrum and angular distribution.[34, 36]

Photoelectron angular distributions for spectral features are characterized by the anisotropy parameter, β. The angular photoelectron intensity, I(θ) is determined by integrating across the full width at half maximum of a feature at different angles, θ of the photoelectron velocity vector and electric vector of the radiation, **ε**. β is obtained by fitting $A[1+\beta P_2(\cos\theta)]$ to I(θ), where *A* is (for these purposes) an arbitrary constant.

Results and Discussion

(CAP)EOM-CCSD Calculation of Low Lying Electronic States

CuF_2^- is a closed shell anion well represented by a single Slater determinant, making the $^1\Sigma_g^+$ ground state a good reference for the EOM-IP-CCSD and EOM-EE-CCSD calculations of the neutral ground, excited anion and excited neutral electronic states relevant to this work. The results of frozen core EOM-CCSD/aug-cc-pVTZ(+3s3p) and, where appropriate, CAP-EOM-CCSD/aug-cc-pVTZ(+3s3p) calculations of the low-lying singlet and doublet electronic states of CuF_2^- and CuF_2 are shown in fig. 2. These adiabatic curves represent cuts along the bending coordinate of the various hypersurfaces at different CuF bond lengths.

Calculations at the Anion Equilibrium Bond Length (1.801 Å)

The curves illustrated in fig. 2a are determined at the anion equilibrium bond length, r(CuF) = 1.801 Å. These show that the minimum on the anion $^1\Sigma_g^+/^1A_1$ ground state surface (black closed circles) corresponds to a linear configuration. $^2\Sigma_g^+/^2A_1$ and $^2\Pi_g/^2B_2$ (black and blue open circles respectively) represent two neutral states (determined via EOM-IP-CCSD). The $^2\Sigma_g^+$ state is 3.542 eV vertically above the anion ground state

minimum while the vertical detachment energy to the $^2\Pi_g$ state is 4.147 eV. At large displacements from linearity the $^2A_1$ and $^2B_2$ states reverse their energy ordering. Strictly the $^2\Pi_g$ state splits into a $^2B_2/^2A_2$ (Mulliken convention, C_{2v} geometry) pair, but for the sake of simplicity only the lower $^2B_2$ component is shown in fig. 2.

At $\angle(FCuF)$=180°, there is a singlet/triplet pair of excited, doubly degenerate anion states which lie vertically above the anion ground state by 3.922 and 3.75 eV respectively - below the $^2\Pi_g$ state but above the $^2\Sigma_g^+$ neutral ground state. Hence these states represent electronic Feshbach-type resonances and are unstable with respect to electron loss. Photoexcitation to the triplet state would represent a spin-forbidden transition and so this state is omitted from fig. 2 and ignored in subsequent discussion. However, the excited singlet state has a profound influence on the CuF_2^- detachment dynamics. Motion along the bending coordinate lifts the degeneracy of this state and it splits into a $^1A_2$ (red, solid circles) and $^1B_2$ (blue, solid circles) pair of states. The maximum in the energies of both at 180° represents a barrier along the bending coordinate at the linear geometry. Upon bending, the energies of both states decrease and cross the neutral $^2A_1$ curve to constitute bound excited anion states. For $\angle(FCuF)$ < 160° ($^1B_2$) and $\angle(FCuF)$ < 155° ($^1A_2$), the curves of fig. 2a are determined using EOM-EE-CCSD. For $\angle(FCuF)$ > 160° ($^1B_2$) and $\angle(FCuF)$ > 155° ($^1A_2$) a CAP-EOM-EE-CCSD treatment is used due to the resonance character. The curves are smoothed in this region to account for discrepancies between the CAP-EOM-CCSD and EOM-CCSD approaches.[37] For the linear geometry the width of the resonance is predicted to be 0.18 eV, but narrows progressively as the states stabilize.

Calculation of Non-linear Isomers

The $^1B_2$ and $^1A_2$ curves show minima along the bending coordinate. These indicate stable, non-linear anion isomers of CuF_2^-. There is a minimum on the $^1B_2$ hypersurface at r(CuF) = 1.823 Å and $\angle(FCuF)$ = 105° in which the electron is vertically bound by 1.568 eV. Fig. 2b shows the energies at this bond length and allows estimation of the adiabatic binding energy (0.406 eV) of the stable $^1B_2$ anion isomer by comparison with fig. 2c which displays the curves at r(CuF) = 1.720 Å. This latter is the calculated (EOM-IP-CCSD) equilibrium bond length of the linear neutral ground state of CuF_2. We note that in the current work our spectra show no evidence of the non-linear anion isomers. However, the calculations raise the possibility that different CuF_2^- isomers could be produced under different ion source conditions.

Calculations at the Neutral Equilibrium Bond Length (1.720 Å)

The global minimum on the neutral ground state potential energy surface is found at r(CuF) = 1.720 Å and $\angle(FCuF)$ = 180°. The linear geometry is in good agreement with previous calculations and experiment. The adiabatic electron affinity (excluding zero-point energy) is 3.369 eV (EOM-IP-CCSD), which compares reasonably with the experimentally measured 3.494 eV. Interestingly, when the anion excited state energies are calculated (as a function of bending angle) at r(CuF) = 1.720 Å the resonances lie slightly above the neutral $^2\Pi_g$ state (at the linear geometry) and thus constitute shape resonances. The width of the $^1\Pi_g$ resonance at this geometry is predicted to be 0.28 eV, i.e. shorter lived and of different character compared to that at the anion equilibrium geometry. Upon bending the $^1A_2$ and $^1B_2$ states drop below the neutral $^2B_2$ state becoming Feshbach resonances before achieving vertical stability with respect to electron loss between 155-150° ($^1B_2$) and 145-140° ($^1A_2$).

In addition to the states discussed above, we note the presence of an anionic state with non-valence character (solid green circles) at bent structures. This state becomes very diffuse as $\angle(FCuF)$ increases and merges with the curve of the neutral ground state at around 150°. Presumably, this corresponds to a virtual state at the linear geometry. However, since CAP-EOM-CCSD is not designed for virtual states, we did not computationally investigate this state further. We have also omitted some higher lying excited anion states which, while they fall into the energy range covered by fig. 2 are inaccessible under the energies employed in the experiments reported later in this work. Nevertheless, fig. 2 shows that there is a rich collection of close lying anion and neutral states associated with CuF_2.

Probing Transient Anion States Via Photoelectron Imaging

In the following results we demonstrate the potential for anion photoelectron imaging to spectroscopically study the short-lived anion states. Estimates based on the symmetric stretching hot-bands suggest (assuming a statistical distribution of energy in the prepared anions) a vibrational temperature sufficient to significantly populate up to 4 quanta in the bending mode.[24] The region of the bending coordinate corresponding to vertical excitation from the (linear) anion (with up to v_{bend} = 4) is illustrated by the grey shading in fig. 2a. The vertical excitation region almost extends to angles at which the resonance becomes bound and hence the resonance width approaches 0 eV. Optical absorption will result in competition between excitation to the detachment continuum associated with the neutral states (direct detachment) and excitation to the quasi-bound anion excited states near the linear configuration, followed by electronic autodetachment. The differences in the selection rules for direct versus auto-detachment lead to different photoelectron transitions appearing in the spectrum. The detachment pathways can be distinguished (to some extent) by the photon energy dependence of the photoelectron spectra and angular distributions which thus provide a probe of the nature and internal structure of the short-lived anion states.

Qualitative prediction of the spectral intensities and photoelectron angular distributions for direct detachment can be made by considering the electronic transition dipole moment ($\left|\langle\psi_{el}\left|\hat{\mu}\right|\psi_i^e\rangle\right|^2$). If we assume the one electron approximation to be valid and that the bound electron (ψ^e), detached electron (ψ_{el}), neutral vibrational (ψ_f^v) and anion vibrational (ψ_i^v) wave functions are separable, detachment

from a σ_g (a_1) orbital gives rise to a laboratory frame photoelectron angular distribution polarized along **ε**. Detachment from a π_g (b_2/a_2) orbital will result in an angular distribution polarized perpendicular to **ε**. The displacements along the normal mode coordinates for the bending (ν_2) and antisymmetric stretching (ν_3) vibrational modes are zero for transitions from the anion ground state to either the $^2\Sigma_g^+$ or $^2\Pi_g$ state meaning the Franck-Condon factors, $\left|\langle\psi_f^{\nu}|\psi_i^{\nu}\rangle\right|^2$ for these modes are zero unless there is zero change in quantum number. However, there is significant displacement along the symmetric stretching (ν_1) mode coordinate which (at sufficient photon energy) gives rise to the appearance of progressions in the spectrum.[24] The photon energy dependence of the allowed direct detachment transitions will be subject to the usual Wigner threshold behaviour, each having low intensity at threshold but gradually increasing as the photon energy increases. In the case of resonance excitation, optical absorption to the $^1A_2$ state is forbidden but excitation of the $^1B_2$ state is possible through the B_2 component of the electronic dipole moment and significant levels of bending excitation can in principle be achieved. In the linear region mixing of the $^1A_2$ and $^1B_2$ states through Renner-Teller vibronic coupling complicates the nature of the excitation. Subsequent to resonance excitation, electronic autodetachment will occur. The appearance of the formally forbidden bending transitions is now possible and the angular distributions of the photoelectrons associated with this mechanism reflect the nature of the excited anion state mediating the detachment processes. The intensity of the bending features in the CuF_2^- spectra is therefore dependent on achieving resonance between the photon energy and the internal levels of the metastable anion states.

Experimental Results

The excitation energy range selected for this work corresponds to the immediate threshold region of the CuF_2^- ($^1\Sigma_g^+$) → CuF_2($^2\Sigma_g^+$) + e^- vibronic band. Calculation suggests that this is significantly below the onset of the CuF_2^- ($^1\Sigma_g^+$) → CuF_2($^2\Pi_g$) + e^- band. We note that in previous work photoexcitation up to 4.005 eV shows no evidence of detachment via the CuF_2($^2\Pi_g$) state.[24]

The photoelectron spectra (fig. 1 shows representative examples) that constitute the raw results of this work were calibrated using F^- detachment. The peaks in the spectra will be referred to as features due to their incorporation of many unresolved transitions. However, the transitions contributing to a given feature tend to have common differences in quantum number. For the most part the unresolved contributions are associated with transitions from a range of bending levels initially populated in the anion ground state.[24] Photoelectron angular distributions, quantified via β, and spectral intensities were monitored as a function of excitation energy for selected features as described in the following sections.

Photoelectron Angular Distributions

The anisotropy parameter, ($-1 \leq \beta \leq +2$) is used to quantify the photon energy dependence of the photoelectron angular distributions of different features. For example, β > 0 indicates maxima in the photoelectron intensity at θ = 0° and 180°, β < 0 indicates greatest intensity at θ = 90°, while β = 0 is an isotropic distribution of photoelectrons. Comparison (and interpretation) of angular distributions between different spectral features is complicated by the eKE dependence of β, the averaging that occurs when two or more transitions overlap and low signal to noise ratios in regions where spectral transitions are weak.

Changes in β as a function of eKE are shown in fig. 3 for several detachment channels. Each data point is taken from an individual feature at a specific photon energy. The open circles are associated with the direct detachment features (1_1^0, black, 0_0^0, red and 1_0^1, blue). The 1_0^1 feature is associated with an eBE of 3.572 eV but is not apparent in the bottom spectrum of fig. 1 due to the proximity to threshold. The filled circles represent features associated with non-zero quanta changes in the bending mode ($2[-2]$, orange, $2[-1]$, green, $2[+1]$, grey, $2[+2]$, yellow, $2[+3]$, purple). For ease of viewing, the solid lines show the data smoothed using a simple three point moving average weighted in the ratio 1:2:1. The contrast between the allowed and forbidden features is clear. 0_0^0, 1_0^1 and 1_1^0 consistently show strongly positive anisotropy parameters consistent with direct detachment via the $^1\Sigma_g^+ \rightarrow {}^2\Sigma_g^+$ transition. The regions of the spectrum associated with changes in the bending quantum number however tend to show much smaller β values, particularly at low eKE. It is true that the anisotropy parameters associated with $2[-2]$, $2[-1]$, and $2[+1]$ show increasingly positive anisotropy values as the eKE increases. However, this is almost certainly due to spectral congestion. Earlier work[24] has shown that at considerably higher photon energy (4.005 eV) the symmetric stretching features have noticeable satellites to slightly lower binding energy. These satellites are associated with direct, zero quanta transitions of the antisymmetric stretching mode ($3_m^{m'=m''}$) and hence produce electrons that are preferentially polarized along **ε**. In the spectra of fig. 1 these are not observed due to proximity to their detachment threshold, but as the photon energy and therefore eKE increases they have a more significant contribution. To reinforce this argument, we note that the 3_1^1 transition has a binding energy of 3.515 eV (only 3 meV different to that of the 2_0^1 transition) and the $1_1^0 3_1^1$ transition has an eBE of 3.453 eV (only 3 meV different to that of the 2_2^0 transition).

Photoelectron Action Spectra

The oscillatory changes in the β values should be correlated with excitation to different internal levels of the resonance(s) mediating autodetachment to bending levels of the neutral. This is not straightforward, but the photoelectron imaging results contain complementary information in the photon energy dependence of the spectral intensities. Within the current limitations of our experimental arrangement it is difficult to efficiently measure the absolute cross section for photodetachment. However, the presence of resolved or

partially resolved structure in the photoelectron spectrum allows determination of relative detachment probabilities. In the following the 0_0^0 feature is used as a reference to determine channel branching ratios, σ. These are constructed by dividing the area under a given spectral feature by that of the 0_0^0 feature. The photon energy dependence of these branching ratios represent action spectra for detachment into the range of transitions associated with each feature.

Fig. 4 shows branching ratios as a function of photon energy for the features associated with changes in the bending mode quantum number. The data are labelled as $2[+1]$ (grey), $2[+2]$ (yellow) and $2[+3]$ (purple). As in fig. 3 the solid lines represent a 1:2:1 weighted moving average to aid viewing of the trends in the data. There are clear oscillations in the branching ratio data, the result of excitation to internal levels of the resonances. Interestingly, the data show several oscillations within the 0.08 eV photon energy range associated with the $2[+1]$ feature. While the widths associated with these oscillations are too broad to allow resolution of rotational structure they must contain information regarding the vibrational structure associated with the CuF_2^- resonances. The observed widths allow a crude estimate of the lifetime (10-100 fs) in the excitation energy range employed, which is in disagreement with the computed width. It is also clear that $2[+1]$ is consistently the most intense of the resonance mediated features and odd numbered changes in bending quanta appear to be favoured over even numbered changes.

On the Nature of the Resonance State(s) Accessed

While it is clear that the observed bending features are mediated by an intermediate anion state, there are (neglecting any change in electron spin) three distinct singlet states that may contribute. These are the $^1A_2/^1B_2$ pair of excited states which have non-linear equilibrium geometries and the virtual $^1A_1$ state hinted at in the calculations. Virtual states are thought to be responsible for observed increases in electron-non-polar molecule scattering cross sections at very low eKE.[38-42] The involvement of a virtual state has some appeal as a way to rationalize our experimental observations. Virtual states are s-wave phenomena, consistent with the isotropic angular distributions associated with the bending features. Additionally, the excitation energies producing the bending features are close to the detachment threshold, again consistent with the properties of virtual states.

The most obvious trends in the resonance mediated spectral features are that changes in bending quantum number clearly occur *and* there is a definite preference for odd numbered changes in bending quanta. This preference does not arise from the autodetachment process itself. The excited anion state must couple with continuum (neutral + electron) states of the same symmetry. In the case of autodetachment the symmetry product of the neutral vibronic and free electron wave functions must match that of the excited anion electronic or vibronic state. However, a symmetry difference is compensated by the symmetry of the photoelectron wave function and all vibronic levels of the neutral ground state are in principle symmetry allowed from an excited anion state.

In the absence of vibronic coupling, transitions between two Σ_g^+ electronic states (such as the anion ground state and virtual state) are symmetry forbidden. Preferential excitation involving odd quanta in the bending mode could arise through vibronic coupling, although in the case of the ground state it is not clear how this would arise as there is no electronic orbital or spin angular momentum to couple with the vibrational angular momentum. A mechanism to inject vibrational excitation would be optical absorption to the non-linear $^1B_2$ state. However, in this scenario there will be no preference for odd/even changes in bending quantum number.

The most likely explanation for the observed behaviour lies in the potential energy variation along the bending coordinate for the $^1B_2/^1A_2$ pair. At the linear geometry the energy reaches a maximum which represents a barrier along the bending coordinate. Additionally, at the maximum these electronic states become degenerate, i.e. they correspond to the components of a $^1\Pi_g$ state which splits as a result of the Renner-Teller effect upon bending. The grey shaded area of fig. 2a shows that photoexcitation from the populated bending levels of the anion ground state accesses the excited state in the region of the barrier. Photon energies sufficient to exceed the barrier will access high levels of vibrational excitation in which there is significant delocalization in the angular coordinate and the anion becomes quasi-linear. This will lead to significant amplitude for the vibrational wave functions in the linear region.[43] Treating excitation from the anion ground state as a $^1\Sigma_g^+ \rightarrow {}^1\Pi_g$ transition, absorption becomes allowed through Renner-Teller interaction with the bending mode. The (u,g) symmetries of the vibronic wave functions will alternate, consistent with the observed preference for odd changes in bending quanta (a parallel is found in CS_2 photoexcitation).[44] The vibronic level structure in this region is likely to be quite complex. The barrier height in fig. 2 only represents a guideline given the adiabatic nature of the potential energy curves, and the vibronic levels will be split by the Renner-Teller interaction. However, it is interesting to note that the bending energy level separations in the non-linear $^1B_2$ state should decrease (due to anharmonicity) as the vibrational energy approaches the barrier top (at $\angle(FCuF)$ = 180°), but as the barrier is exceeded the bending level separation will increase.[45] This is qualitatively consistent with the emergence of more clearly defined structure in the 2[+1] and 2[+3] branching ratio data at the higher end of the excitation energy range.

Conclusions

In summary, experimental results (branching ratios and photoelectron angular distributions) recorded in narrowly spaced energy intervals reveal details of both direct and resonance mediated transitions. Despite the transient nature of the excited anion states, the branching ratio data represent action spectra that depend on the vibronic structure of the resonance(s). The *ab initio* calculations, albeit neglecting non-adiabatic coupling between the electronic states of the

system, provide clues as to the nature of the resonances. To treat interacting resonance states, linear vibronic coupling models were developed many years ago.[46, 47] Corresponding models within the CAP-EOM-CCSD framework are currently under development and need to be adapted to the present case to fully interpret the experimental data.[48] At the same time, the ability to experimentally probe photodetachment yields and link photon energy dependent variations to particular detachment channels provides important benchmarks for current and future theoretical work.

Conflicts of interest

There are no conflicts to declare.

Acknowledgements

Acknowledgements are made for the support of this work by the National Science Foundation (RM under CHE – 1566157), Deutsche Foschungsgemeinschaft, grant JA 2794/1-1 (Emmy Noether program) (TJ).

References

1 N. Moiseyev, *Non-Hermitian quantum mechanics*, Cambridge University Press, Cambridge, UK, 2011.
2 S. Klaiman and I. Gilary, *Adv. Quantum Chem.*, 2012, **63**, 1-31.
3 J. Simons, *Ann. Rev. Phys. Chem.*, 2011, **62**, 107-128.
4 J. Simons, *J. Phys. Chem. A*, 2008, **112**, 6401-6511.
5 J. Simons, in *Photoionization and Photodetachment*, ed. C. Y. Ng, World Scientific Publishing Co., Singapore, 2000, pp. 959-1010.
6 K. D. Jordan and P. D. Burrow, *Chem. Rev.*, 1987, **87**, 557-558.
7 K. D. Jordan, V. K. Voora and J. Simons, *Theor. Chim. Acta*, 2014, **133**, 1445.
8 B. Boudaïffa, P. Cloutier, D. Hunting, M. A. Huels and L. Sanche, *Science*, 2000, **287**, 1658-1660.
9 J. Simons, *Acc. Chem. Res.*, 2006, **39**, 772-779.
10 R. Santra and L. S. Cederbaum, *Phys. Rep.*, 2002, **368**, 1-117.
11 J. G. Muga, J. P. Palao, B. Navarro and I. L. Egusquiza, *Phys. Rep.*, 2004, **395**, 357-426.
12 U. V. Riss and H. D. Meyer, *J. Phys. B*, 1993, **26**, 4503-4535.
13 T. C. Jagau and A. I. Krylov, *J. Phys. Chem. Lett.*, 2014, **5**, 3078-3085.
14 T. C. Jagau, D. Zuev, K. B. Bravaya, E. Epifanovsky and A. I. Krylov, *J. Phys. Chem. Lett.*, 2014, **5**, 310-315.
15 U. V. Riss and H. D. Meyer, *J. Phys. B*, 1995, **28**, 1475-1493.
16 U. V. Riss and H. D. Meyer, *J. Phys. B*, 1998, **31**, 2279-2304.
17 N. Moiseyev, *J. Phys. B*, 1998, **31**, 1431-1441.
18 D. B. Dao and R. Mabbs, *J. Chem. Phys.*, 2014, **141**, 154304.
19 T. C. Jagau, D. B. Dao, N. Holtgrewe, A. I. Krylov and R. Mabbs, *J. Phys. Chem. Lett.*, 2015, **6**, 2786-2793.
20 M. Van Duzor, J. Wei, F. Mbaiwa and R. Mabbs, *J. Chem. Phys.*, 2010, **133**, 144303.
21 M. Van Duzor, F. Mbaiwa, J. Lasinski, N. Holtgrewe and R. Mabbs, *J. Chem. Phys.*, 2011, **134**, 214301.
22 D. W. Chandler and P. L. Houston, *J. Chem. Phys.*, 1987, **87**, 1445-1447.
23 A. T. J. B. Eppink and D. H. Parker, *Rev. Sci. Instrum.*, 1997, **68**, 3477-3484.
24 J. Lyle, S. R.C., J. R. Hamilton, B. A. Traylor, T. L. Guasco, T. C. Jagau and R. Mabbs, *J. Chem. Phys.*, 2018, **149**, 084302.
25 K. R. Lykke, D. M. Neumark, T. Andersen, V. J. Trapa and W. C. Lineberger, *J. Chem. Phys.*, 1987, **87**, 6842-6853.
26 D. M. Wetzel and J. I. Brauman, *J. Chem. Phys.*, 1989, **90**, 68-73.
27 J. Marks, D. M. Wetzel, P. B. Comita and J. I. Brauman, *J. Chem. Phys.*, 1986, **84**.
28 J. Lyle, O. Wedig, S. Gulania, A. I. Krylov and R. Mabbs, *J. Chem. Phys.*, 2017, **147**, 234309.
29 F. Mbaiwa, M. Van Duzor, J. Wei and R. Mabbs, *J. Phys. Chem. A*, 2010, **114**, 1539-1547.
30 D. L. Osborn, D. J. Leahy, D. M. Cyr and D. M. Neumark, *J. Chem. Phys.*, 1996, **104**, 5026-5039.
31 W. C. Wiley and I. H. McLaren, *Rev. Sci. Instrum.*, 1955, **26**, 1150-1157.
32 B. Y. Chang, R. C. Hoetzlein, J. A. Mueller, J. D. Geiser and P. L. Houston, *Rev. Sci. Instr.*, 1998, **69**, 1665-1670.
33 L. Wen, S. D. Chambreau, S. A. Lahankar, A. Sridhar and A. Suits, *Rev. Sci. Instrum.*, 2005, **76**, 063106.
34 J. Lyle, S. R. Chandramoulee, C. A. Hart and R. Mabbs, *J. Vis. Exp.*, 2018, **137**, e57989.
35 V. Dribinski, A. Ossadtchi, V. A. Mandelshtam and H. Reisler, *Rev. Sci. Instrum.*, 2002, **73**, 2634-2642.
36 C. E. Moore, *Atomic Energy Levels as Derived from the Analysis of Optical Spectra – Volume I. The spectra of hydrogenm deuterium, tritium, helium, lithium, beryllium, boron, carbon, nitrogen, oxygen, fluorine, neon, sodium, magnesium, aluminum, silicon, phosphorus, sulfur, chlorine, argon, potassium, calcium, scandium, titanium, and vanadium*, NSRDS-NBS 35, 1971.
37 Z. Benda and T. C. Jagau, *J. Chem. Theory Comput.*, 2018, 4216-4223.
38 D. Field, J. P. Ziesel, S. L. Lunt, R. Parathasarathy, L. Suess, S. B. Hill, F. B. Dunning, R. R. Lucchese and F. A. Gianturco, *J. Phys. B*, 2001, **34**, 4371-4381.
39 W. Vanroose, C. W. McCurdy and T. N. Rescigno, *Phys. Rev. A*, 2002, **66**, 032720.
40 D. Field, N. C. Jones and J. P. Ziesel, *Phys. Rev. A*, 2004, **69**, 052716.
41 N. C. Jones, D. Field and J. P. Ziesel, *J. Chem. Phys.*, 2005, **122**, 074301.
42 A. S. Barbosa and M. H. F. Bettega, *J. Chem. Phys.*, 2017, **146**, 154302.
43 W. Quapp and B. P. Winnewisser, *Journal of Mathematical Chemistry*, 1993, **14**, 259-285.
44 K. O. Lantz, V. Vaida and J. Donaldson, *Chem. Phys. Lett.*, 1991, **184**, 152-158.
45 R. N. Dixon, *J. Phys. Colloques*, 1971, **32**, 147-154.
46 H. Estrada, L. S. Cederbaum and W. Domcke, *J. Chem. Phys.*, 1986, **84**, 152-169.

47 S. Feuerbacher, T. Sommerfeld and L. S. Cederbaum, *J. Chem. Phys.*, 2004, **120**, 3201-3214.
48 Z. Benda and T. C. Jagau, *J. Phys. Chem. Lett.*, 2018.

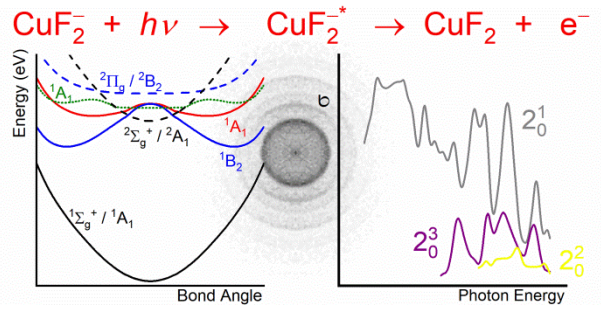

Internal level structure of temporary anion states (resonances) are probed using action spectroscopy obtained from photoelectron imaging of CuF_2^-.

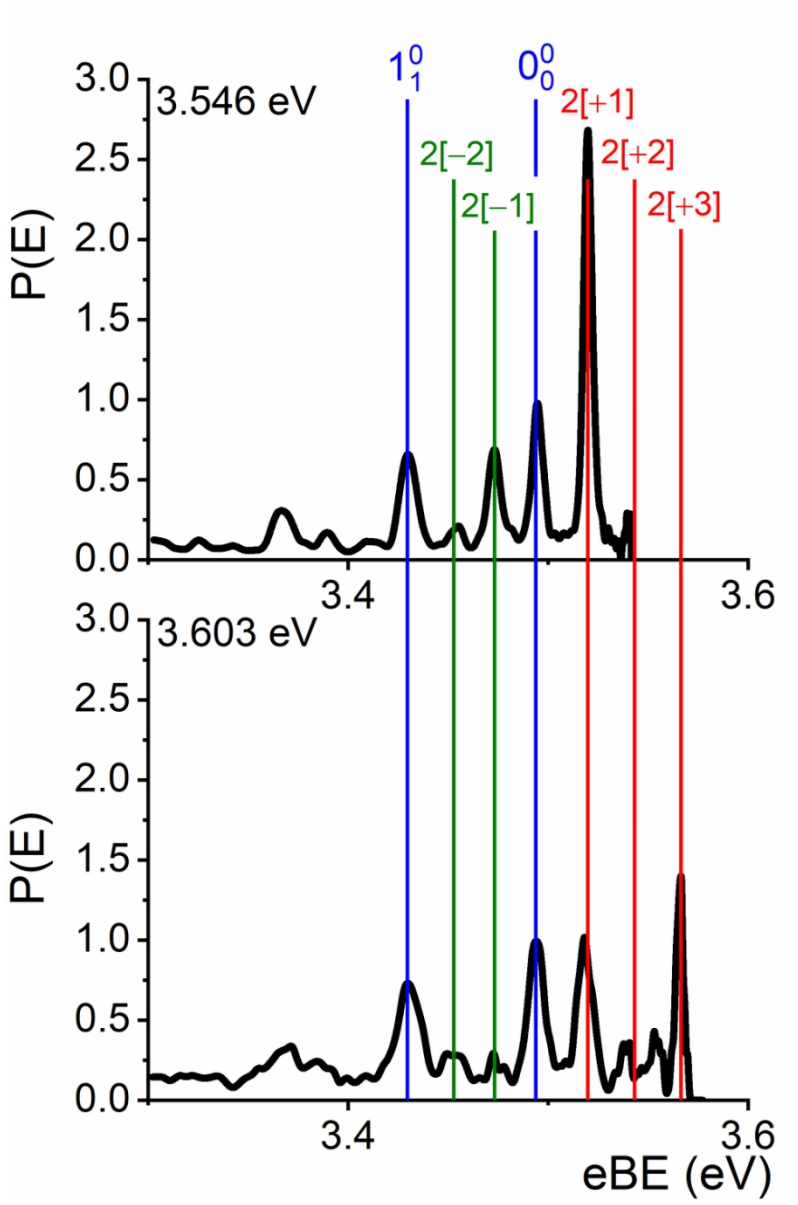

Fig. 1: Representative photoelectron spectra recorded at photon energies 3.546 eV (top) and 3.603 eV (bottom). The spectral assignments are discussed in the text.

83x127mm (300 x 300 DPI)

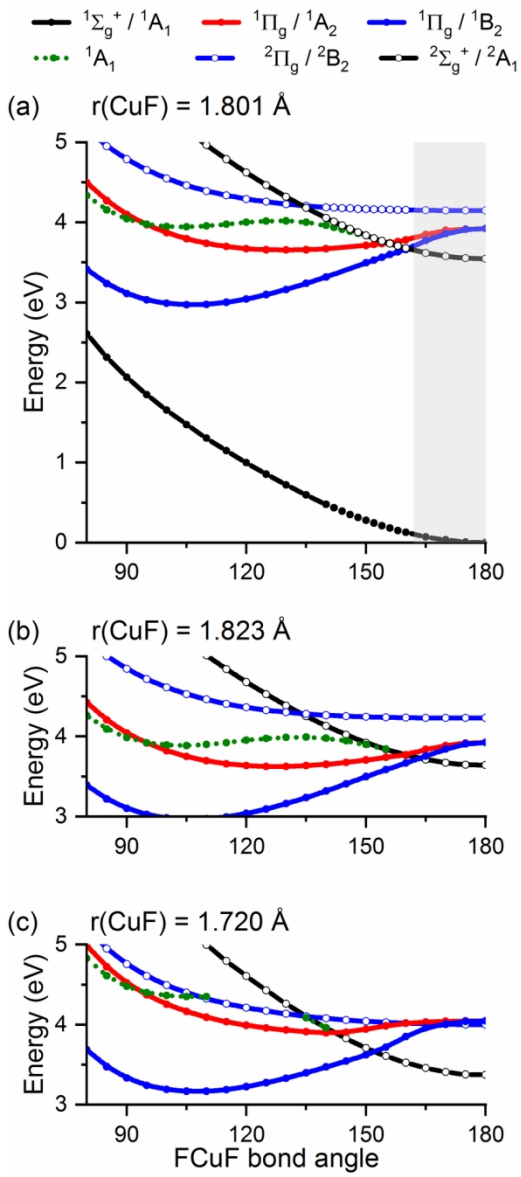

Fig. 2: Adiabatic potential energy curves along the bending coordinate for the low-lying singlet and doublet states of the CuF_2 anion and neutral systems. Curves are shown at the equilibrium bond lengths of (a) the anion ground state, (b) the $^1B_2$ state, and (c) the neutral ground state.

76x178mm (300 x 300 DPI)

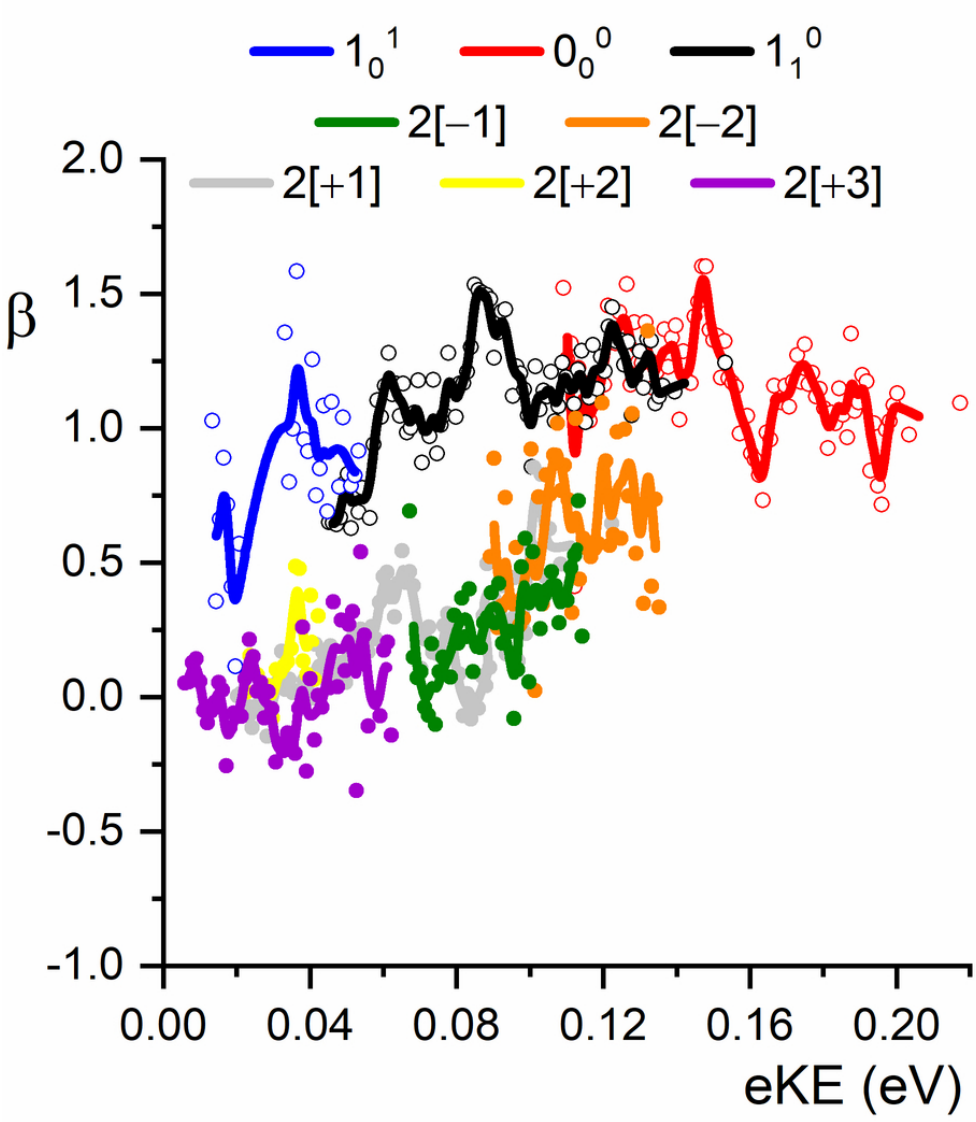

Fig. 3: Variation in β with eKE for various features in the CuF_2^- photoelectron spectrum. Each point for a given feature represents a particular photon energy. The closed circles refer to features dominated by changes in the bending quantum number. Open circles refer to features in which there is no change in bending quantum number. The solid lines serve as a guide to the eye (see text for details).

78x88mm (300 x 300 DPI)

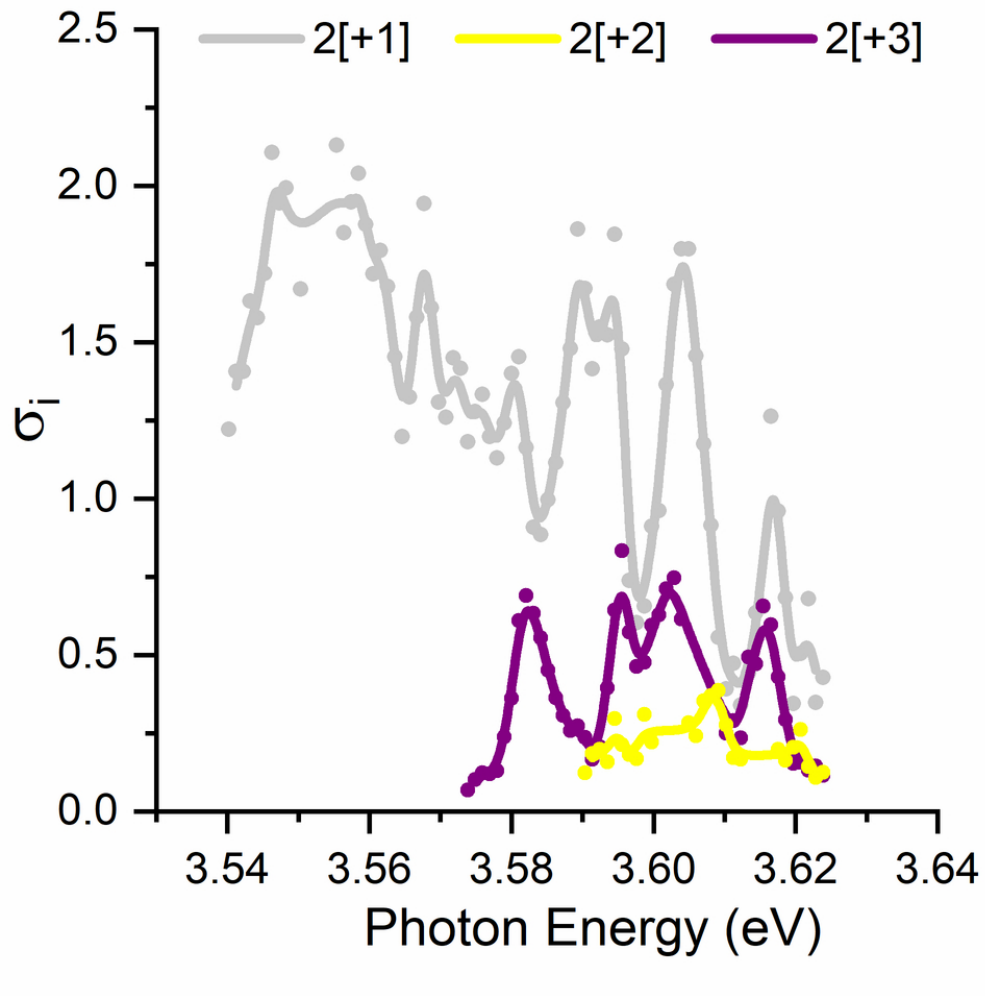

Fig. 4: Branching ratios for spectral features involving an increase in bending quantum number. Each data point is recorded at a particular photon energy. The solid lines serve as a guide to the eye (see text for details).

81x81mm (300 x 300 DPI)